PAPER

Check for updates

Electrochemical synthesis of NiCo layered double hydroxides on nickel-coated graphite for water splitting: understanding the electrochemical experimental parameters†

Patrick Marcel Seumo Tchekwagep, [iD] *[abc] Craig E. Banks, [iD] [d] Robert D. Crapnell, [iD] [d] Murat Farsak[e] and Gülfeza Kardaş *[a]

The electrochemical synthesis of nickel–cobalt (Ni–Co) layered double hydroxides (LDHs) on a nickel-coated graphite support for water splitting applications was investigated. Three different electrochemical approaches, namely, cyclic voltammetry (CV), chronoamperometry (CA), and chronopotentiometry (CP), were employed for evaluating the electrodeposition of Ni–Co LDHs. The graphite support was initially coated with a thin layer of Ni by applying 50 mA cm^{-2} constant current density for 120 s. Raman spectroscopy results confirmed the intercalation of nitrates, evidenced by the characteristic Raman bands at 1033 cm^{-1} (v_1) and 1329 cm^{-1} (v_3). These characteristic bands were indicative of nitrate intercalation, a key feature of LDHs, further supporting the classification of the synthesized material as NiCo LDHs on a nickel-coated graphite support. It was observed that the electrochemical routes used for the synthesis influenced the morphology, composition, and electrochemical behavior of the obtained Ni–Co LDHs. Moreover, atomic force microscopy (AFM) measurements revealed distinct nanoscale surface characteristics associated with the synthesis methods, with the Ni–Co LDH synthesized *via* the CV route exhibiting higher surface heterogeneity than that synthesized *via* the constant potential method (CA), resulting in a more textured surface. These findings were further supported by roughness average (Ra) values, where CV-synthesized Ni–Co LDH displayed the highest R_a of 221 nm, indicating a more extensive active surface area. The electrochemical performance, both for the hydrogen evolution reaction (HER) and oxygen evolution reaction (OER), were correlated with these surface variations. This study provides valuable insights into the electrochemical experimental parameters for the synthesis of Ni–Co LDHs and their potential application in water splitting processes.

Introduction

According to the United Nations, the size of the global population is projected to reach 8.8 billion in 2030 and will continue rising to around 9.7 billion in 2050 and 10.9 billion in 2100.[1] This continuous growth of population will intrinsically induce an increase in the energy demand to meet the needs of people for transportation, heating, cooling, lighting and other activities. As fossil fuels have been the dominant source of energy for human societies for centuries,[2] meeting this demand will likely require continued reliance on these resources.

However, because of the potentially catastrophic effects of human-caused greenhouse gas emissions, along with the fact there is only a finite amount of fossil fuels, there is an urgent need to reduce our dependence on fossil fuels. Among new ways to power our lives without destroying the planet, hydrogen energy has been regarded as one of the cleanest when renewable energy sources, including solar, and wind, are used for water electrolysis.[3,4]

Currently, the efficiency and the cost-effectiveness of water electrolysis for hydrogen production remain challenging, and it is less competitive than other methods such as hydrogen production from fossil fuels through steam reforming.[5] However, research and development efforts are ongoing to improve the efficiency of the process and reduce the cost of materials and equipment.[6–8]

[a]Chemistry Department, Faculty of Arts and Sciences, Çukurova University, 01330 Balcalı, Adana, Turkiye. E-mail: 3omues@gmail.com; gulfeza@cu.edu.tr

[b]Applied Chemistry and Biosciences Laboratory, Department of Chemistry-Biology, Faculty of Science, University of Bertoua, Bertoua 416, Cameroon

[c]Analytical Chemistry Laboratory, Faculty of Science, University of Yaoundé 1, Yaoundé 812, Cameroon

[d]Faculty of Science and Engineering, Manchester Metropolitan University, Dalton building, Chester Street, M1 5GD, UK

[e]Department of Battery Systems and Hydrogen Technologies, Osmaniye Korkut Ata University, Institute of Natural and Applied Science, Turkiye

† Electronic supplementary information (ESI) available. See DOI: https://doi.org/10.1039/d4ra08053j

In general, proton exchange membrane (PEM) and alkaline water electrolysers are two commonly used systems for producing hydrogen through the electrolysis of water.[9] While PEM water electrolysers can offer a higher hydrogen production rate, it is limited by the high cost of efficient membranes and catalysts, which are precious metals.[10] Operating under alkaline conditions offers an alternative to using expensive catalysts, such as from the platinum group, as it promotes the use of cheaper and essentially non-precious metals, leading to the production of hydrogen at a lower cost.[11]

To produce cost-effective hydrogen through water electrolysis, the focus can be on designing efficient and inexpensive electrocatalysts. Thus, the hydrogen evolution reaction (HER) and oxygen evolution reaction (OER) will occur at a minimal overpotential, given that the reversible potential to split water is 1.23 V.

Among various materials, 3d transition metal-based layered double hydroxides (LDHs) containing different metals such as nickel, cobalt, and iron are promising electrocatalysts due to their flexibility in the composition, readily structure and morphology modulation (unique lamellar structure), tunable thickness and layer spacing, and abundant active sites.[12–14] LDHs can be synthesized using various chemical methods, including co-precipitation,[15,16] hydrothermal,[17,18] sol–gel[19,20] and urea hydrolysis,[21,22] and can be produced as either thin films or powders. These chemical methods are often time-consuming and complex, and the resulting powdered materials typically require the addition of binders, which often decrease the performance. To skip the use of binders and tune directly the surface of the electrode, electrochemistry techniques stand as elegant options that are facile, rapid and scalable.

In their review, Mousty and Walcarius highlighted the use of electrochemically assisted local pH tuning as an effective approach for the deposition of thin films of LDHs, driven by electrogenerated hydroxide anions at the electrode surface.[23] In a recent review, Rohit et al. provide a detailed electrodeposition mechanism behind the formation of LDHs with nucleation and growth processes and provide an extensive summary of the literature on electrodeposited LDH-based electrode materials on energy and environmental applications.[24] Based on insights from that review, we identified 89 papers, out of the 121 used, in this study that specifically focus on the electrosynthesis of LDHs. These papers were categorized according to the explored applications of LDHs and the electrodeposition methods employed. The extracted information is then summarized in Fig. 1. It can be noticed that chronopotentiometry, chronoamperometry and cyclic voltammetry are the most common techniques used for electrodeposition of LDHs on a given support.

From Fig. 1, one can see that chronoamperometry is by far the most used technique followed by cyclic voltammetry. Regarding HER and OER applications, only 16% of LDHs have been synthesized using cyclic voltammetry and 68% using chronoamperometry. While these works explore the electrodeposition of LDHs and NiCo hydroxides in broad terms, they do not specifically address the electrodeposition of NiCo LDHs for electrocatalytic water splitting. Our study narrows this focus by
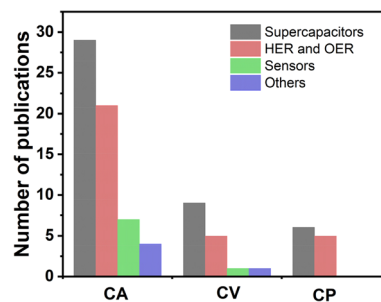

Fig. 1 Histogram for the number of publications on the synthesis of LDHs used for various applications using chronoamperometry (CA), cyclic voltammetry (CV) and chronopotentiometry (CP).

investigating the influence of the electrochemical routes on NiCo LDHs synthesis and highlighting their performance in hydrogen and oxygen evolution reaction applications.

Experimental section

Materials (chemicals used)

All chemicals were of analytical grade and used as received. All solutions were prepared with double distilled water. $Ni(NO_3)_2 \cdot 6H_2O$ ($\geq$98%) was purchased from Carl Roth GmbH, $Co(NO_3)_2 \cdot 6H_2O$ was purchased from Carlo Erba. KOH ($\geq$84%), $NiSO_4 \cdot 6H_2O$ ($\geq$98%), $NiCl_2 \cdot 6H_2O$ ($\geq$98%) and H_3BO_3 ($\geq$99.5%) were purchased from Merck.

Modification of graphite with nickel and NiCo layered double hydroxide catalysts

Prior to the deposition of nickel on the graphite support, graphite (Ø 0.6 cm) was mechanically polished with emery paper P600. The polished electrode was ultrasonicated in a mixture (1 : 5 v/v) ethanol–water bath for 5 min and thoroughly rinsed with double distilled water. The electrode was used for further modifications directly after cleaning.

The deposition of nickel on graphite was performed using a potentiostat/galvanostat CHI660D electrochemical workstation. A 2-electrode cell configuration was used for electrodeposition. A nickel plate (3.8 cm × 4.8 cm × 0.15 cm) was used as a counter and reference electrode, whereas graphite (0.28 cm²) was used as a working electrode. Electrodeposition was carried out by applying 50 mA cm^{-2} for 120 s under a stirred solution of nickel bath containing 30% $NiSO_4 \cdot 6H_2O$, 1% $NiCl_2 \cdot 6H_2O$ and 1.25% H_3BO_3. The obtained electrode denoted as Ni-GP was rinsed thoroughly with water and directly used for both, electrochemical measurements and further modifications.

The electrosynthesis of NiCo LDH was performed using a standard 3-electrode set-up connected to a potentiostat/galvanostat CHI660D electrochemical workstation. A platinum sheet (1 cm × 1 cm × 0.1 cm) was used as a counter electrode, Ag/AgCl (3 M KCl) as the reference electrode and Ni-GP as the working electrode. A freshly prepared 0.025 M solution containing Co^{2+} and Ni^{2+} at a molar ratio of 1 : 1 was used as an electrolyte. Electrodeposition was carried out by scanning at the range of −1.2 V to 0.2 V$_{Ag/AgCl}$ and back at 5 mV s^{-1} scan rate

potential (one cycle) by applying − 1.0 $V_{Ag/AgCl}$ for 120 s and by applying 1 mA cm^{-2} for 300 s for cyclic voltammetry, chronoamperometry and chronopotentiometry, respectively. After the modification the obtained electrode, denoted as NiCo–OH–Ni-GP, was thoroughly rinsed with water and immediately used for electrochemical measurements.

Characterization of the catalyst

Electrochemical impedance spectroscopy (EIS) measurements were recorded at an amplitude of 10 mV and frequency range of 10^6–10^{-1} Hz in 1.0 M KOH. Before performing EIS, the open circuit potential was monitored for 5 min. After EIS measurements, linear sweep voltammetry (LSV) was performed from −1.0 to −1.6 $V_{Ag/AgCl}$ and 0.4 to 0.8 $V_{Ag/AgCl}$ at a scan rate 1 mV s^{-1} for hydrogen evolution reaction (HER) and oxygen evolution reaction (OER), respectively. Lastly, cyclic voltammetry (CV) was performed from −1.6 to 0.6 $V_{Ag/AgCl}$ and back at a scan rate of 50 mV s^{-1}. Electrochemical measurements of graphite and the modified graphites were performed in 1.0 M KOH at room temperature.

After the modification of the graphite electrode, Scanning Electron Microscopy (SEM) analysis was performed using a FEI, Model: 650 Field Emission SEM equipped with energy-dispersive X-ray spectroscopy (EDX) to investigate the film's morphology and elemental composition. The crystalline phase of the film deposited on graphite was examined by performing X-ray Diffraction (XRD) analysis using the PANalytical Model: EMPYREAN XRD instrument. Raman spectra were recorded with the Renishaw Model: in *Via* Qontor instrument by employing an argon laser tuned at 532 nm. For Fourier Transform Infrared (FTIR) spectroscopy, a Nicolet iS10 FTIR 142 spectrometer from Thermo Scientific was used, employing the Attenuated Total Reflection (ATR) technique. For a detailed examination of the film's surface topography and roughness, Atomic Force Microscopy (AFM) was employed using the Park System Model: Park NX10 instrument.

Results and discussion

Electrodeposition of Ni and NiCo-LDH

Electrochemical deposition of the first layer of nickel was achieved by applying a constant current at the electrode surface. According to Nasispouri,[25] the resulting chronopotentiometry curve (Fig. 2a) can be divided into two distinct portions: the first corresponds to nucleation, occurring within the first 20 s, while the second corresponds to a stable potential and the growth of previously formed nuclei. During this process, hydrogen gas is formed alongside the target reaction of nickel ion reduction. The mechanism can be explained by the following electrochemical reactions:
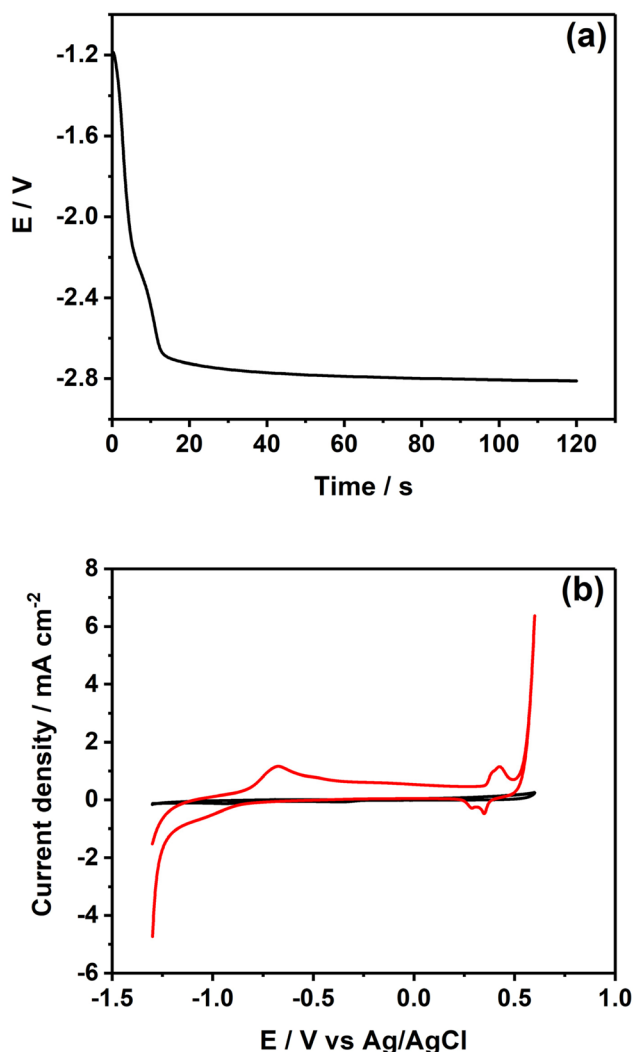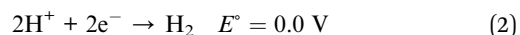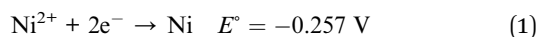
$$Ni^{2+} + 2e^- \rightarrow Ni \quad E° = -0.257 \text{ V} \quad (1)$$

$$2H^+ + 2e^- \rightarrow H_2 \quad E° = 0.0 \text{ V} \quad (2)$$

Fig. 2 (a) Schematic for the electrodeposition of Ni on the graphite electrode using chronopotentiometry at 50 mA cm^{-2} for 120 s. (b) Cyclic voltammograms on the bare graphite (black curve) and nickel-coated graphite (red curve) recorded in 1.0 M KOH at 50 mV s^{-1}.

According to Faraday's law and assuming that the current efficiency is 100%, the thickness of the deposited film can be estimated at approximately 2 μm thickness. Fig. 2b displays the cyclic voltammograms obtained for graphite and nickel-coated graphite electrodes. It is evident that the modified electrode exhibits the characteristic feature of nickel between 0 and 0.6 $V_{Ag/AgCl}$, as demonstrated in eqn (3).

$$Ni(OH)_2 + OH^- \leftrightarrow NiOOH + H_2O + e^- \quad (3)$$

Furthermore, the increase in capacitive current provides additional evidence of the successful modification of the graphite surface with nickel.

Electrochemical deposition of NiCo–OH film was performed by scanning through the oxidation potentials and back (Fig. 3a), at a constant cathodic potential (Fig. 3b) and a constant cathodic current density (Fig. 3c). Negative polarization induced the reduction of nitrate ions, which generated hydroxides (eqn
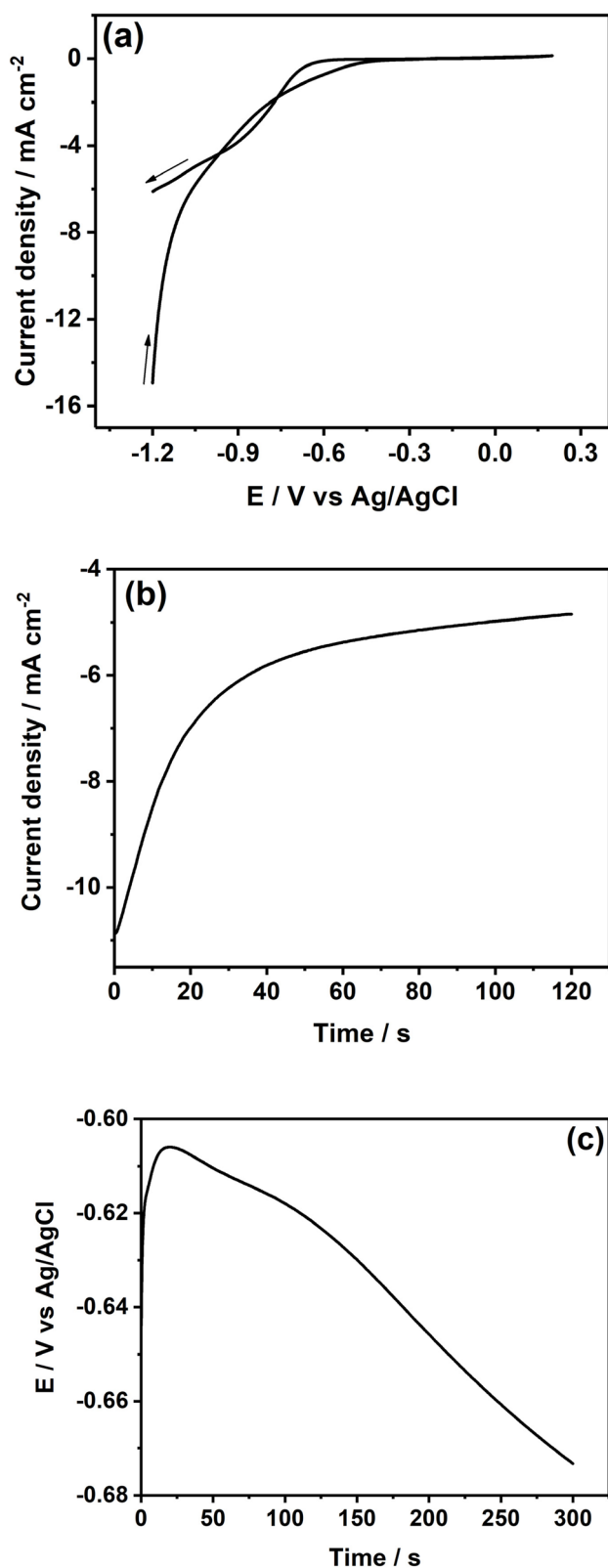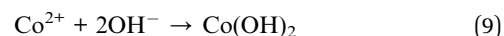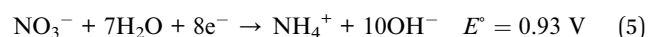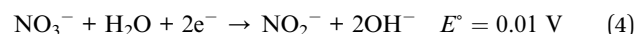
Fig. 3 Electrodeposition on Ni-GP using (a) cyclic voltammetry at 5 mV s⁻¹ from −1.2 V to 0.2 V and back (b) chronoamperometry at −1.0 V for 120 s and (c) chronopotentiometry at 1.0 mA cm⁻² for 300 s in a solution containing 0.025 M Co^{2+} and Ni^{2+} at a molar ratio 1 : 1.

(4) and (5)). These hydroxides coprecipitated the nickel and cobalt to give nickel and cobalt hydroxide (eqn (7)).[26–28] However, side reactions may also occur, including the production of individual hydroxides from nickel (eqn (8)) and cobalt (eqn (9)), as well as the reduction of water (eqn (6)). The hydrogen generated from the reduction of water *via* these side reactions may damage the LDH formed on the electrode surface.[29,30]

The hydroxides formed tend to diffuse towards the solution during the electrochemical deposition process, while the metallic cations diffuse from the solution to the electrode surface.

$$NO_3^- + H_2O + 2e^- \rightarrow NO_2^- + 2OH^- \quad E° = 0.01 \text{ V} \quad (4)$$

$$NO_3^- + 7H_2O + 8e^- \rightarrow NH_4^+ + 10OH^- \quad E° = 0.93 \text{ V} \quad (5)$$

$$2H_2O + 2e^- \leftrightarrow H_2 + 2OH^- \quad E° = -0.83 \text{ V} \quad (6)$$

$$xNi^{2+} + yCo^{2+} + (2x + 2y)OH^- \rightarrow Ni_xCo_yOH_{(2x+2y)} \quad (7)$$

$$Ni^{2+} + 2OH^- \rightarrow Ni(OH)_2 \quad (8)$$

$$Co^{2+} + 2OH^- \rightarrow Co(OH)_2 \quad (9)$$

The observed decrease in the current and potential instability over time while scanning (Fig. 3b and c) suggests the growth of insulating material (NiCo LDH) on the graphite surface. Based on our observations, it is likely that with one cycle (Fig. 3a), 120 s (Fig. 3b) and 300 s (Fig. 3c), the amount of the material deposited on the electrode surface is relatively small.

Electrochemical characterization

To gain insights into each modification step, electrochemical impedance spectroscopy was employed to conduct the electrochemical characterization of graphite and modified graphite electrodes at the open circuit potential. The Nyquist plots shown in Fig. 4a reveal that differences between each electrode are relatively minor; however, it is evident that the electrode material obtained *via* cyclic voltammetry (CV) exhibits a lower polarization resistance compared to the materials produced by chronoamperometry (CA) and chronopotentiometry (CP). The polarization resistance obtained from the Nyquist plot at OCP can provide insights into the ease of the charge transfer at the electrode/electrolyte interface. This is reflected in the fitted polarization resistance (R_2) values: 41 245 Ω for CV, 45 621 Ω for CA, and 49 004 Ω for CP. The lower R_2 for the CV electrode indicates the enhanced electron transfer kinetics, likely due to favorable surface properties or higher catalytic activity, which may improve its suitability for applications requiring efficient charge transfer. Furthermore, all systems show a consistently low electrolyte resistance (R_1), approximately 5.1 Ω, suggesting that the variations in the performance are primarily due to differences in the electrode surface characteristics in the solution. This uniformity in R_1 highlights that the differences in the charge transfer resistance (R_2) are intrinsic to the electrode materials themselves.
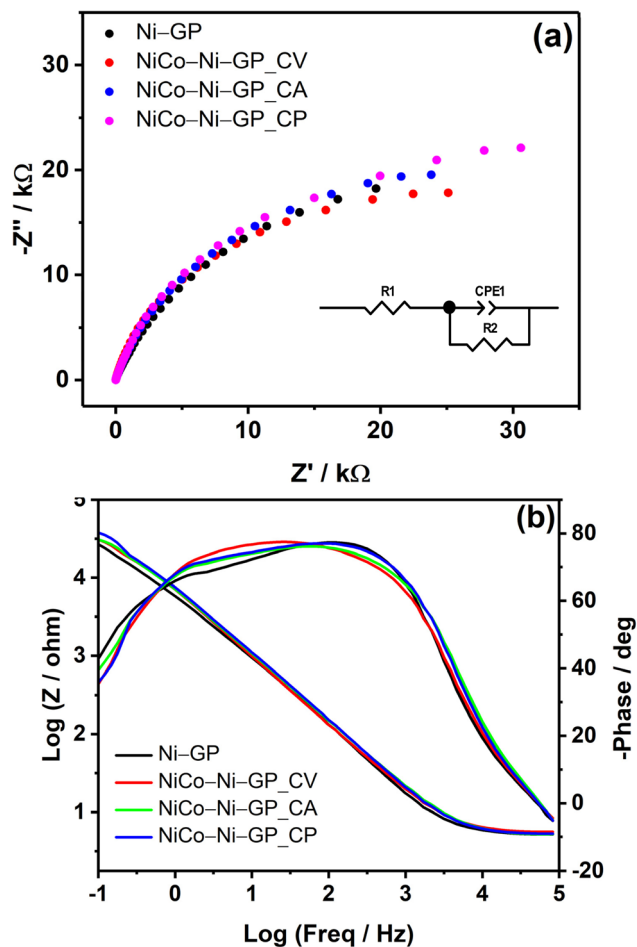
Fig. 4 (a) Nyquist and (b) Bode plots of graphite modified with Ni and NiCo–OH electrodeposited (using different routes) on graphite coated with Ni at OCP.

Moreover, the EIS presented in the Bode plot format (Fig. 4b) clearly shows that the electrodeposition of NiCo LDH onto the electrodeposited Ni/graphite electrode leads to an increase in the polarization resistance (from 26 791 Ω to 37 757 Ω), confirming that LDH impedes the current flow, as also observed in Fig. 3b with the decrease of the current density during the electrodeposition of NiCo LDH. A porous catalyst structure enhances double-layer capacitance, leading to a more pronounced negative phase angle, which is seen at around −80° at the mid-frequency region. This phenomenon indicates faster charge transfer kinetics, reducing polarization resistance, which is essential for efficient catalysis. At the high-frequency region of the Bode phase plots, the phase angle tends to 0°. Such responses are typical of uncompensated resistance, which in this experiment will predominantly be due to the solution resistance through the electrolyte (R_s). The distribution of the Bode modulus for the different electrodes displays a similar trend of the correlation between $|Z|$ and frequency.

Additionally, it can also be noticed that the trend in the polarization resistance values from the Bode plot matches with those obtained from the fitting process. For instance, the highest polarization resistance of 37 757 Ω corresponds to the
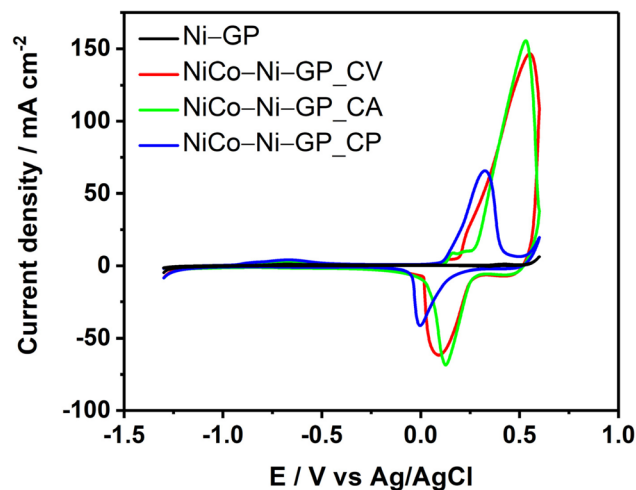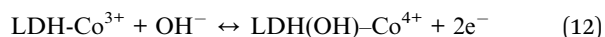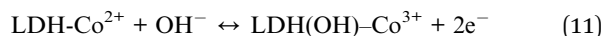

Fig. 5 Cyclic voltammograms of a graphite electrode modified with Ni and NiCo−OH electrodeposited using different routes; recorded in 1.0 M KOH at 50 mV s^{-1}.

LDH electrodeposited using CP. Furthermore, at higher frequencies, the solution resistance is approximately 5.2 Ω, which is in good agreement with the value derived from the fitting.

Fig. 5 depicts the cyclic voltammograms recorded with the different electrodes. In contrast to EIS characterization, cyclic voltammograms display many features for each electrode and they are mainly between −0.2 V to +0.6 V. The total oxidation charge is higher for the material obtained with CV and CA, indicating that a larger amount of material is deposited on the surface. The small current density used (1 mA cm^{-2}) may explain the small oxidation charge resulting from a small amount of the material deposited on the electrode material.

Additionally, the majority of the material obtained through CV undergoes oxidation at a higher oxidation potential than that obtained through CA and CP, which could be attributed to the presence of Ni and Co, as suggested by eqn (10)–(12).[29,30]

$$LDH\text{-}Ni^{2+} + OH^- \leftrightarrow LDH(OH)\text{-}Ni^{3+} + 2e^- \qquad (10)$$

$$LDH\text{-}Co^{2+} + OH^- \leftrightarrow LDH(OH)\text{-}Co^{3+} + 2e^- \qquad (11)$$

$$LDH\text{-}Co^{3+} + OH^- \leftrightarrow LDH(OH)\text{-}Co^{4+} + 2e^- \qquad (12)$$

At this level of the study, we could have an explanation of the discrepancy between the oxidation charge, which is higher than the reduction charge. This could be attributed to the loss of material or/and material, which is partially reversible while scanning back towards reduction potential.

SEM-EDX, XRD and Raman characterization

Upon visual inspection, distinct colors were observed for the electrodeposited films on graphite (Photo 1S†). To gain more insights into the surface structure and composition, SEM-EDX was conducted. SEM images showed significant differences in the structure obtained using the synthesis technique. For the
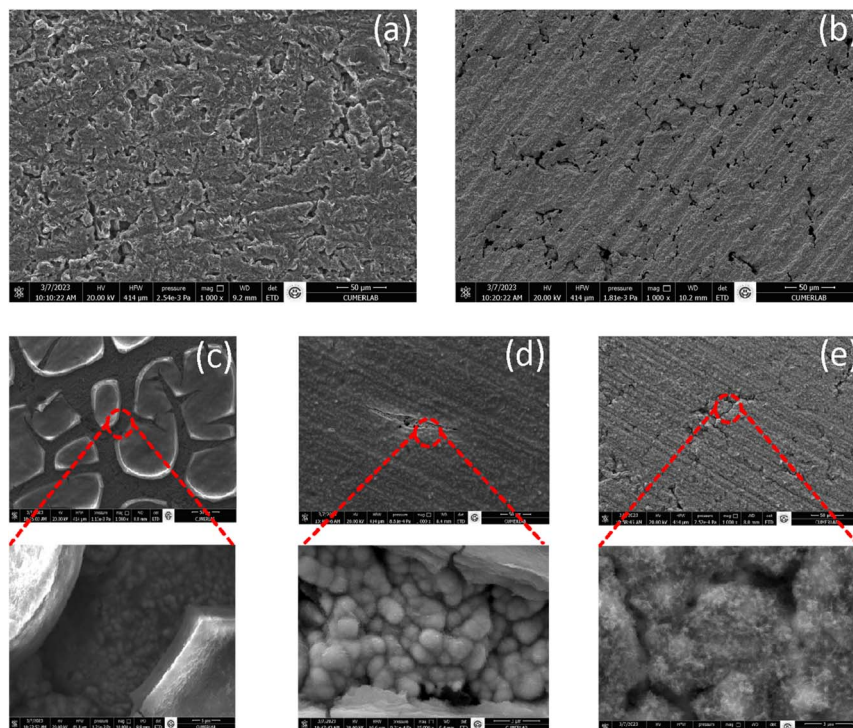
Fig. 6 SEM micrographs of (a) graphite, (b) Ni modified graphite, (c) graphite coated with Ni modified with NiCo−OH using cyclic voltammetry, (d) chronoamperometry, and (e) chronopotentiometry.

nickel synthesis, particle aggregation was observed on the graphite surface with an even distribution. However, some holes were also observed, likely due to the production of hydrogen gas during the deposition of nickel (Fig. 6b). EDX examination revealed that the film composition after the electrodeposition of nickel contained 93% nickel and possibly a partial oxide, as evidenced by the presence of about 2% oxygen in the film composition (Table 1).

The SEM image of the material obtained with CV showed fractal portions of material given a partial coverage of the nickel layer (Fig. 6c). Here more edges of the material are exposed and probably increase the surface area of the active material.

Table 1 Composition of graphite, Ni-modified graphite, and graphite coated with Ni modified with NiCo−OH using cyclic voltammetry, chronoamperometry and chronopotentiometry determined by EDX analysis

Material	Composition (weight %) in film				
	C	O	Ni	Co	Rest
GP	97.03	2.97			
GP/Ni	4.63	1.83	92.53		1.01
GP/Ni/NiCo LDH-CV[a]	5.19	19.04	69.47	6.3	
GP/Ni/NiCo LDH-CV	4.75	38.48	29.23	27.54	
GP/Ni/NiCo LDH-CA[a]	4.61	6.72	86.68	1.54	0.45
GP/Ni/NiCo LDH-CA	4.64	34.97	38.78	21.61	
GP/Ni/NiCo LDH-CP	6.44	24.03	56.91	12.15	0.47

[a] The probe was located where the film was cracked.

For the film obtained with CA, one can observe that the layer of nickel is more covered with a film having a spindle-like cut (Fig. 6d) offering fewer edges of the main material exposed. Note that the LDH film appeared like a uniformly laid plastic film upon a nickel layer. Lastly, the film obtained using CP exhibited a uniform layer with a network-like structure, as illustrated in the magnified image in Fig. 6e.

EDX analysis was performed at different locations on the film, revealing a Ni/Co ratio of 1 : 1 for the LDH film synthesized with CV (Table 1), which is consistent with the metal ratio in the synthesis solution. These findings are in line with the studies conducted by Musella *et al.*, which demonstrated that the potentiodynamic method enables the synthesis of LDH films with a controlled composition using different ratios of Fe^{3+} or Al^{3+} to Co^{2+} cations in the electrolytic solution.[29] When the analysis was performed in the cracks (magnified image, Fig. 6c) or the spindle-like cut (magnified image, Fig. 6d), a higher percentage of nickel was detected, indicating that this region corresponds to the first nickel layer synthesized. However, the percentage of oxygen in that region may imply the presence of individual hydroxides of nickel and cobalt. For the LDH film obtained with CA, the Ni/Co was approximately 2 : 1, and for CP it was 5 : 1, which does not match the ratio of cations in the bath solution. This suggests that there is a disparity in the rate of hydroxide production, leading to the coprecipitation of nickel and cobalt at different rates. Controlling the overpotential with CA provides good control over the thermodynamics and kinetics of the system,[29,30] but the resulting composition suggests that the rate of hydroxide production is not precisely controlled. On

the other hand, applying a constant current between the working electrode (Ni/GP) and the counter electrode allows for better control over the rate of hydroxide production compared to the potentiostatic technique. This is because the current is directly related to the rate of ion transfer at the electrode surface and thus the rate of OH⁻ production. By maintaining a constant current, the rate of OH⁻ production can be kept stable and uniform. However, to ensure proper operation of the potentiostat, the applied potential must be adjusted during the deposition. This can lead to difficulties in controlling the side processes during electrodeposition, which may result in a difference between the molar ratio of Ni/Co in the bath solution and in the structure formed. During cyclic voltammetry, the scanning from the reduction potential towards the oxidation potential may result in faster nucleation and growth of the LDH film. However, scanning at a slow rate, there is more time for the nickel and cobalt ions species to diffuse from the bulk solution to the electrode surface, while allowing for a steady and uniform production of hydroxide at the electrode surface. This results in the formation of a thick layer of LDH. Additionally, dewetting effects can lead to the formation of voids or defects in the film, which, in this case, appear to improve the performance of the resulting material, as will be discussed in the next section.

XRD analysis was performed directly on different electrodes. The resulting patterns were predominantly characterized by the pattern of graphite (as shown in Fig. 7), with the (002) peak being the most intense at 26.2°. Additionally, the (110), (004) and (006) planes were observed at 42.2°, 54.2° and 77.4°, respectively. For the nickel patterns, the most intense peak was observed at 44.4° for the (111) plane, followed by peaks at 51.8° for the (200) plane and 76.3° for the (220) plane. Importantly, the absence of the typical peak corresponding to the (111) reflection of NiO crystal structure at around 37.2° confirmed the low proportion of the oxide, as further supported by the EDX analysis.

Unfortunately, we observed a poor expression of the typical peak at 11.1°, which corresponds to the basal spacing between the LDH layers for the (003) plane. The better definition of the
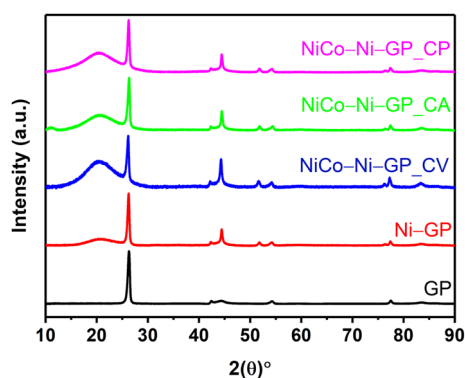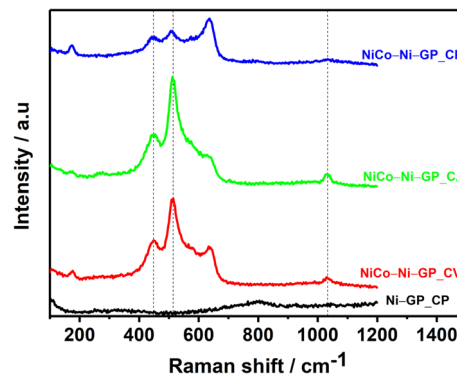

Fig. 8 Raman spectra of the nickel modified graphite screen-printed electrode and Ni-modified graphite screen-printed electrode coated with NiCo−OH using cyclic voltammetry (CV), chronoamperometry (CA), and chronopotentiometry (CP).

peak at 20.5° might be attributed to the (006) plane and corresponds to the interlayer distance between the LDHs layers. The absence of the peak for the (003) plane in the material obtained with CP could be explained by a poor crystallization of the LDH formed.

While the characteristic peak at 10°, indicative of the layered double hydroxides (LDHs), is not prominently evident in the XRD pattern, it is assumed that this may be attributed to the relatively thin film or the presence of a less well-defined crystal structure, resulting in low crystallinity. The electrochemical conditions employed for electrodeposition, possibly lead to the formation of a very thin film, which could contribute to the observed XRD pattern.

In the literature, the acquisition of a typical LDH XRD pattern often involves performing cyclic voltammetry for a minimum of two cycles and utilizing longer deposition times through chronoamperometry or chronopotentiometry.[26,30,31] However, despite the subtle XRD features, Raman spectroscopy provides clear evidence of the presence of NiCo LDH on the electrode, as illustrated in Fig. 8.

Comparing our Raman results with those from existing literature, the main spectral features of NiCo LDH include well-defined peaks at 448 and 514 cm⁻¹, corresponding to the vibrational modes of Ni–O and Co–O, respectively.[29,31–33] Furthermore, the Raman band at 1033 cm⁻¹ is assigned to the symmetric stretching (ν_1) of the intercalated nitrates. This assignment is supported by the observation of the ν_3 stretching mode of the nitrates at 1329 cm⁻¹ in the infrared spectrum of the electrodeposited NiCo LDHs, as depicted in Fig. S1.† As well, the absorption peak at 634 cm⁻¹ can be assigned to M–O, O–M–O, and M–O–M (M = Co and Ni) vibrations.[33,34]

Electrocatalytic activity in 1 M KOH

In this section, we explore the electrocatalytic performance of the materials synthesized *via* electrodeposition towards both, the hydrogen evolution reaction (HER) and oxygen evolution reaction (OER) in 1.0 M KOH. Fig. 9 shows typical linear sweep voltammograms obtained for GP, Ni-GP and NiCo–Ni-GP. In terms of HER, the onset potentials were found to be −1.30,

Fig. 7 XRD patterns of the as-obtained graphite, Ni-modified graphite, and the graphite coated with Ni modified with NiCo−OH using cyclic voltammetry, chronoamperometry, and chronopotentiometry.
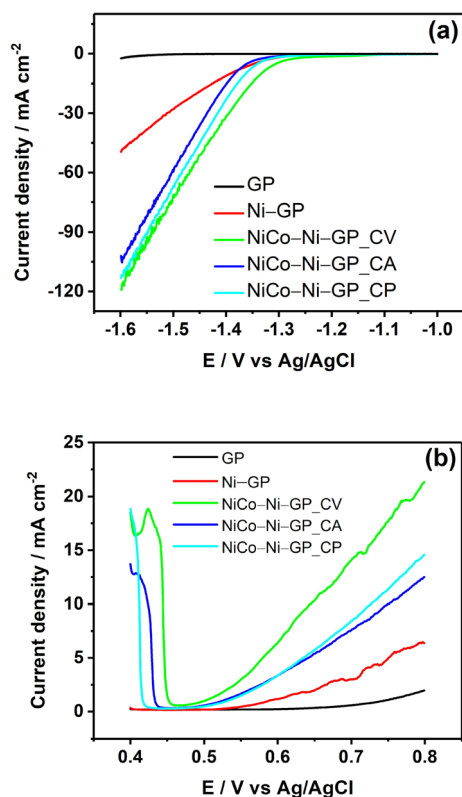
Fig. 9 Variation of (a) HER and (b) OER activity of NiCo−OH obtained using different electrosynthesis routes. The measurements were performed in 1.0 M KOH at a scan rate potential of 1.0 mV s^{-1}.

−1.32 and −1.36 $V_{Ag/AgCl}$ for LDH electrodeposited using CV, CP and CA, respectively. This shows that the NiCo–Ni-GP produced *via* cyclic voltammetry gave rise to a lower overpotential.

Using the data presented in Fig. 9A, we performed a Tafel analysis for LDH electrodeposited using CV, we observed a Tafel slope of 22.5 mV dec^{-1}, which shows that the predominate step is following the Tafel reaction and further investigation is needed.

It is worth noting that LDH obtained using CV and having a Ni/Co ratio of 1 : 1 shows better electrocatalytic activity towards HER and OER. This enhanced performance can be attributed to the specific structure and composition of CV-LDH. In a similar trend, Musella *et al.* have demonstrated that films of Ni/Al-LDH and Co/Al-LDH electrodeposited using a potentiodynamic route exhibit better stability, reproducibility and superior performance for supercapacitor application.[29] Additionally, Gualandi *et al.* showed that Ni/Al-LDH electro-synthesized using a potentiodynamic approach exhibits higher sensibility when used as an electrode material for glucose sensing.[30] Supplementing our analysis with Atomic Force Microscopy (AFM) measurements, our study provides additional insights into the nanoscale topography and surface roughness of NiCo LDH materials synthesized through different electrochemical approaches, as illustrated in Fig. 10.

AFM images reveal distinct surface characteristics associated with various synthesis methods. Specifically, the NiCo LDH material obtained *via* CV exhibits a higher degree of surface heterogeneity, while the material synthesized using the CA method displays a more uniform surface. The roughness of the surfaces, quantified by the roughness average (R_a), reflects these differences. The NiCo LDH material obtained through CV exhibits the highest R_a value, measuring 221 nm, indicating a more textured surface. In contrast, the R_a values for the materials obtained through constant current (CP) and constant potential (CA) are 90 nm and 30 nm, respectively. These findings suggest that the material synthesized *via* CV offers a larger
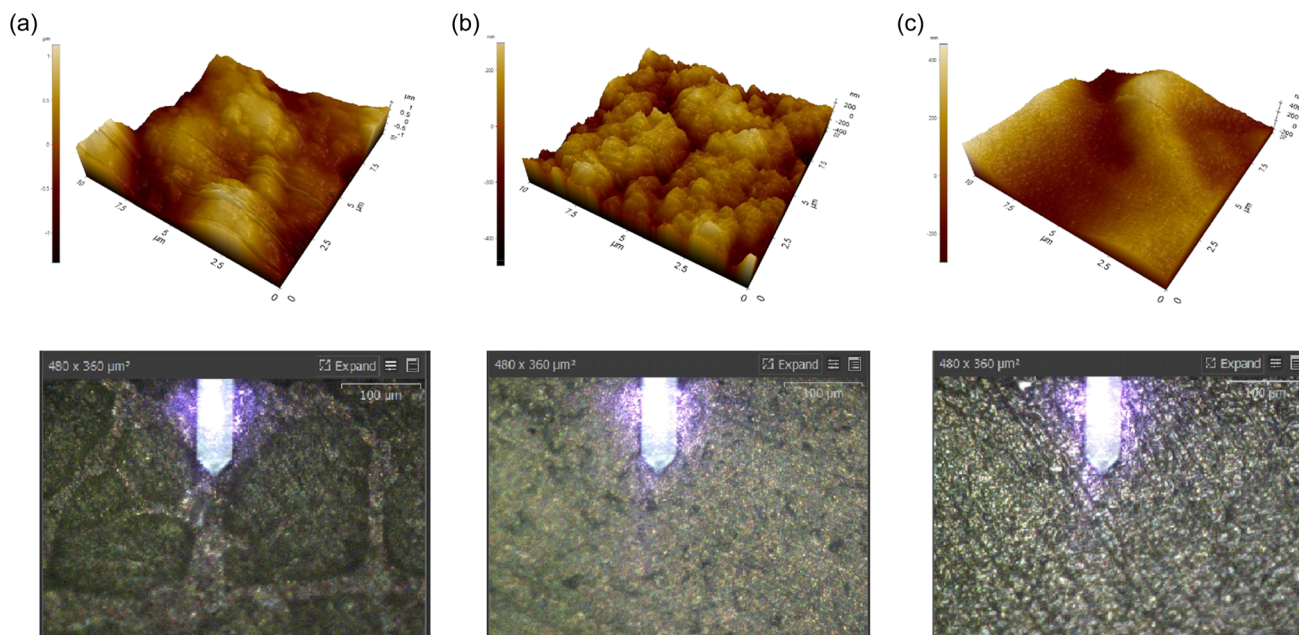

Fig. 10 3D and 2D AFM images of the graphite surface coated with Ni modified with NiCo−OH using (a) cyclic voltammetry (CV), left, (b) chronopotentiometry (CP), middle and (c) chronoamperometry (CA), right.

active surface area, correlating with its superior electrocatalytic performance in both the hydrogen evolution reaction (HER) and the oxygen evolution reaction (OER). Importantly, these surface characteristics revealed by AFM align with and are corroborated with electrochemical measurements. In fact, by integrating the reduction peaks in the cyclic voltammograms (Fig. 5), we obtained charge values (Q_{red}) of 33.14 mC, 26.90 mC and 21.49 mC for NiCo LDH electrodeposited with CV, CA and CP, respectively. Considering that the charge is intrinsically related to the flow of electrons and, thus, to the active surface, it can be affirmed that the material obtained using CV contains a more significant active surface area compared to the material obtained using CA and CP.

Conclusions

In summary, we explored the electrochemical synthesis of NiCo layered double hydroxides (LDHs) on nickel-coated graphite substrates. Our primary aim was to unravel the intricate relationship between electrochemical parameters and the properties of obtained NiCo LDHs. Our findings shed light on the nuanced distinctions among the LDHs synthesized using different electrochemical methods. Notably, cyclic voltammetry emerged as a promising route, yielding layered double hydroxides with a balanced 1 : 1 Ni/Co ratio. These materials exhibited noteworthy electrocatalytic activity for hydrogen and oxygen evolution reactions. This suggests that cyclic voltammetry might hold potential for designing efficient LDH electrocatalysts.

Data availability

The data supporting this article have been included as part of the ESI.†

Conflicts of interest

There are no conflicts to declare.

Acknowledgements

References

1 United Nations Department of Economic and Social Affairs, Population Division, *World Population Prospects 2022: Summary of Results*, 2022, UN DESA/POP/2022/TR/NO. 3.

2 J. L. Holechek, H. M. E. Geli, M. N. Sawalhah and R. Valdez, A Global Assessment: Can Renewable Energy Replace Fossil Fuels by 2050?, *Sustainability*, 2022, **14**, 4792.

3 M. van der Spek, C. Banet, C. Bauer, P. Gabrielli, W. Goldthorpe, M. Mazzotti, S. T. Munkejord, N. A. Røkke, N. Shah, N. Sunny, D. Sutter, J. M. Trusler and M. Gazzani, Perspective on the hydrogen economy as a pathway to reach net-zero CO_2 emissions in Europe, *Energy Environ. Sci.*, 2022, **15**, 1034–1077.

4 S. G. Nnabuifea, E. Oko, B. Kuang, A. Bello, A. P. Onwualu, S. Oyagha and J. Whidborne, The Prospects of Hydrogen in Achieving Net Zero Emissions by 2050: A Critical Review, Sust, *Chem. Clim. Action*, 2023, **5**, 100072.

5 A. Badgett, M. Ruth, B. James and B. Pivovar, Methods identifying cost reduction potential for water electrolysis systems, *Curr. Opin. Chem. Eng.*, 2021, **33**, 100714.

6 J. Hao, K. Wu, C. Lyu, Y. Yang, H. Wu, J. Liu, N. Liu, W. Lau and J. Zheng, Recent advances in interface engineering of Fe/Co/Ni-based heterostructure electrocatalysts for water splitting, *Mater. Horiz.*, 2023, **10**, 2312–2342.

7 A. Raveendran, M. Chandran and R. Dhanusuraman, A comprehensive review on the electrochemical parameters and recent material development of electrochemical water splitting electrocatalysts, *RSC Adv.*, 2023, **13**, 3843–3876.

8 A. Ali, F. Long and P. K. Shen, Innovative Strategies for Overall Water Splitting Using Nanostructured Transition Metal Electrocatalysts, *Electrochem. Energy Rev.*, 2022, **5**, 1.

9 S. S. Kumar and H. Lim, An overview of water electrolysis technologies for green hydrogen production, *Energy Rep.*, 2022, **8**, 13793–13813.

10 K. Ayers, High efficiency PEM water electrolysis: enabled by advanced catalysts, membranes, and processes, *Curr. Opin. Chem. Eng.*, 2021, **33**, 100719.

11 M. David, C. Ocampo-Martínez and R. Sánchez-Peña, Advances in alkaline water electrolyzers: A review, *J. Energy Storage*, 2019, **23**, 392–403.

12 Z. Cai, X. Bu, P. Wang, J. C. Ho, J. Yang and X. Wang, Recent advances in layered double hydroxide electrocatalysts for the oxygen evolution reaction, *J. Mater. Chem. A*, 2019, 7, 5069–5089.

13 Q. Chen, Y. Yu, J. Li, H. Nan, S. Luo, C. Jia, P. Deng, S. Zhong and X. Tian, Recent Progress in Layered Double Hydroxide-Based Electrocatalyst for Hydrogen Evolution Reaction, *Chemelectrochem*, 2022, **9**, e202101387.

14 Y. Wang, M. Zhang, Y. Liu, Z. Zheng, B. Liu, M. Chen, G. Guan and K. Yan, Recent Advances on Transition-Metal-Based Layered Double Hydroxides Nanosheets for Electrocatalytic Energy Conversion, *Adv. Sci.*, 2023, **10**, 2207519.

15 H. L. Tcheumi, A. P. K. Wendji, I. K. Tonle and E. Ngameni, A Low-Cost Layered Double Hydroxide (LDH) Based Amperometric Sensor for the Detection of Isoproturon in Water Using Carbon Paste Modified Electrode, *J. Anal. Methods Chem.*, 2020, **2020**, 8068137.

16 S. Mallakpour, M. Hatami and C. M. Hussain, Recent innovations in functionalized layered double hydroxides: Fabrication, characterization, and industrial applications, *Adv. Colloid Interface Sci.*, 2020, **283**, 102216.

17 M. Duan, S. Liu, Q. Jiang, X. Guo, J. Zhang and S. Xiong, Recent progress on preparation and applications of layered double hydroxides, *Chin. Chem. Lett.*, 2022, **33**, 4428–4436.

18 Q. Qian, G. Yu, Q. Zhao and X. Zhang, One-step hydrothermal preparation of bilayer films of NiCo LDH/Pt

loaded on nickel foam surface for HER catalytic activity, *New J. Chem.*, 2023, **47**, 1040–1044.

19 L. Valeikiene, R. Paitian, I. Grigoraviciute-Puroniene, K. Ishikawa and A. Kareiva, Transition metal substitution effects in sol-gel derived $Mg_{3-x}M_x/Al_1$ (M=Mn, Co, Ni, Cu, Zn) layered double hydroxides, *Mater. Chem. Phys.*, 2019, **237**, 121863.

20 A. Smalenskaite, M. M. Kaba, I. Grigoraviciute-Puroniene, L. Mikoliunaite, A. Zarkov, R. Ramanauskas, I. A. Morkan and A. Kareiva, Sol–Gel Synthesis and Characterization of Coatings of Mg-Al Layered Double Hydroxides, *Materials*, 2019, **12**, 3738.

21 S. Naseem, B. Gevers, R. Boldt, F. J. W. J. Labuschagne and A. Leuteritz, Comparison of transition metal (Fe, Co, Ni, Cu, and Zn) containing tri-metal layered double hydroxides (LDHs) prepared by urea hydrolysis, *RSC Adv.*, 2019, **9**, 3030–3040.

22 S. Nayak and K. Parida, Plethora of preparatory features on single layered double hydroxide towards energy conversion process, *Mater. Res. Bull.*, 2023, **162**, 112185.

23 C. Mousty and A. Walcarius, Electrochemically assisted deposition by local pH tuning: a versatile tool to generate ordered mesoporous silica thin films and layered double hydroxide materials, *J. Solid State Electrochem.*, 2015, **19**, 1905.

24 R. C. Rohit, A. D. Jagadale, S. K. Shinde and D.-Y. Kim, A review on electrodeposited layered double hydroxides for energy and environmental applications, *Mater. Today Commun.*, 2021, **27**, 102275.

25 F. Nasirpouri, Fundamentals and principles of electrode-position, in *Electrodeposition of Nanostructured Materials*, Springer Series in Surface Sciences, vol. 62, Springer, Cham, 2017, pp. 75–121.

26 I. Gualandi, M. Monti, E. Scavetta, D. Tonelli, V. Prevot and C. Mousty, Electrodeposition of Layered Double Hydroxides on platinum: Insights into the reactions sequence, *Electrochim. Acta*, 2015, **152**, 75–83.

27 X. Lu and C. Zhao, Electrodeposition of hierarchically structured three-dimensional nickel–iron electrodes for efficient oxygen evolution at high current densities, *Nat. Commun.*, 2015, **6**, 6616.

28 M. Shao, R. Zhang, Z. Li, M. Wei, D. G. Evans and X. Duan, Layered double hydroxides toward electrochemical energy storage and conversion: design, synthesis and applications, *Chem. Commun.*, 2015, **51**, 15880–15893.

29 E. Musella, I. Gualandi, M. Giorgetti, E. Scavetta, F. Basile, A. Rivalta, E. Venuti, F. Corticelli, M. Christian, V. Morandi and D. Tonelli, Electrosynthesis and characterization of Layered Double Hydroxides on different supports, *Appl. Clay Sci.*, 2021, **202**, 105949.

30 I. Gualandi, Y. Vlamidis, L. Mazzei, E. Musella, M. Giorgetti, M. Christian, V. Morandi, E. Scavetta and D. Tonelli, Ni/Al Layered Double Hydroxide and Carbon Nanomaterial Composites for Glucose Sensing, *ACS Appl. Nano Mater.*, 2019, **2**, 143–155.

31 E. Musella, I. Gualandi, E. Scavetta, M. Gazzano, A. Rivalta, E. Venuti, M. Christian, V. Morandi and D. Tonelli, Electrochemical Approach for the Production of Layered Double Hydroxides with a Well-Defined Co/Me^{III} Ratio, *Chem.–Eur. J.*, 2019, **25**, 16301–16310.

32 E. Musella, I. Gualandi, E. Scavetta, A. Rivalta, E. Venuti, M. Christian, V. Morandi, A. Mullaliu, M. Giorgetti and D. Tonelli, Newly developed electrochemical synthesis of Co-based Layered Double Hydroxides: toward noble metal-free electro-catalysis, *J. Mater. Chem. A*, 2019, **7**, 11241–11249.

33 X. Cai, X. Shen, L. Ma, Z. Ji, C. Xu and A. Yuan, Solvothermal synthesis of NiCo-layered double hydroxide nanosheets decorated on RGO sheets for high performance supercapacitor, *Chem. Eng. J.*, 2015, **268**, 251–259.

34 R. Li, Z. Hu, X. Shao, P. Cheng, S. Li, W. Yu, W. Lin and D. Yuan, Large Scale Synthesis of NiCo Layered Double Hydroxides for Superior Asymmetric Electrochemical Capacitor, *Sci. Rep.*, 2016, **6**, 18737.